Atmos. Chem. Phys. Discuss., 14, 24311–24348, 2014
www.atmos-chem-phys-discuss.net/14/24311/2014/
doi:10.5194/acpd-14-24311-2014

Atmospheric Chemistry and Physics Discussions

Recent satellite-based trends of tropospheric nitrogen dioxide over large urban agglomerations worldwide

P. Schneider[1], **W. A. Lahoz**[1], **and R. van der A**[2]

[1]NILU – Norwegian Institute for Air Research, P.O. Box 100, 2027 Kjeller, Norway
[2]Royal Netherlands Meteorological Institute (KNMI), P.O. Box 201, 3730 AE De Bilt, the Netherlands

Received: 2 July 2014 – Accepted: 28 August 2014 – Published: 19 September 2014

Correspondence to: P. Schneider (ps@nilu.no)

Published by Copernicus Publications on behalf of the European Geosciences Union.

Abstract

Trends in tropospheric nitrogen dioxide (NO_2) concentrations over 66 large urban agglomerations worldwide have been computed using data from the SCanning Imaging Absorption spectroMeter for Atmospheric CHartographY (SCIAMACHY) instrument onboard the Envisat platform for the period August 2002 to March 2012. A seasonal model including a linear trend was fitted to the satellite-based time series over each site. The results indicate distinct spatial patterns in trends. While agglomerations in Europe, North America, and some locations in East Asia/Oceania show decreasing tropospheric NO_2 levels on the order of $-5\,\%\,yr^{-1}$, rapidly increasing levels of tropospheric NO_2 are found for agglomerations in large parts of Asia, Africa, and South America. The site with the most rapidly increasing absolute levels of tropospheric NO_2 was found to be Tianjin in China with a trend value of $3.04(\pm0.47)\times10^{15}$ molecules $cm^{-2}\,yr^{-1}$, whereas the site with the most rapidly increasing relative trend was Kabul in Afghanistan with $14.3(\pm2.2)\,\%\,yr^{-1}$. In total, 34 sites exhibited increasing trends of tropospheric NO_2 throughout the study period, 24 of which were found to be statistically significant. A total of 32 sites showed decreasing levels of tropospheric NO_2 during the study period, of which 20 sites did so at statistically significant magnitudes. Overall, going beyond the relatively small set of megacities investigated previously, this study provides the first consistent analysis of recent changes in tropospheric NO_2 levels over most large urban agglomerations worldwide.

1 Introduction

More than half of the world's population now lives in urban areas. Megacities, i.e. cities with more than 10 million inhabitants, as well as other large urban agglomerations have seen rapid growth over the last decades and this trend is expected to continue in the near future (United Nations, 2012a). The number of megacities is expected to rise from currently 23 to a total of 37 megacities in the year 2025 (Zhu et al., 2012).

ACPD
14, 24311–24348, 2014

Such large urban agglomerations exhibit intensive human activities and high levels of energy consumption. This leads to strongly increased emissions of a wide variety of air pollutants and greenhouse gases, severely affecting both air quality and climate (Mage et al., 1996; Mayer, 1999; Fenger, 1999; Molina and Molina, 2004; Molina et al., 2004; Gurjar et al., 2008; Chan and Yao, 2008; Monks et al., 2009; Gurjar et al., 2010; Baklanov et al., 2010; Parrish et al., 2011; Kanakidou et al., 2011; Cassiani et al., 2013).

Nitrogen dioxide (NO_2) is one of the major air pollutants and is strongly related to population density. As such it is a significant environmental issue in many large urban agglomerations (Schneider and van der A, 2012; Lamsal et al., 2013; Hilboll et al., 2013). However, station observations of NO_2 are relatively rare on a global scale, and in particular in developing countries, and thus are not able to provide a global and spatially continuous perspective. Satellite observations on the other hand offer a unique opportunity for studying the spatial and temporal dynamics of tropospheric NO_2 (Richter et al., 2005; van der A et al., 2008; Schneider and van der A, 2012; Hilboll et al., 2013).

Furthermore, satellite observations of atmospheric composition are a very important part of operational chemical weather forecasting as it is for example carried out by the Copernicus Atmosphere Monitoring Service (http://atmosphere.copernicus.eu/), which uses data assimilation techniques (Lahoz and Schneider, 2014) to make the best use of the satellite information of atmospheric composition (Flemming et al., 2009; Inness et al., 2013). The Copernicus Atmosphere Monitoring Service is being developed within the framework of a series of EU-funded research projects, the latest of them being the Monitoring Atmospheric Composition and Climate – Interim Implementation (MACC-II). Within the MACC-II project, a subproject on input data (OBS) organizes, structures, and evaluates input data. As part of this work, the feasibility of using SCanning Imaging Absorption spectroMeter for Atmospheric CartograpHY (SCIAMACHY) data for estimating trends in tropospheric NO_2 was investigated and is reported on here.

Going beyond trends determined over actual megacities as done in previous studies (Schneider and van der A, 2012; Hilboll et al., 2013), we present here the first detailed

ACPD
14, 24311–24348, 2014

satellite-based global analysis of tropospheric NO_2 trends for a significantly expanded set of of large urban agglomerations worldwide. The trends are derived from a consistent and homogeneous satellite time series for the period from August 2002 through March 2012, making use of the full archive of SCIAMACHY data.

The manuscript is structured as follows: Sect. 2 summarizes the current state of knowledge with respect to global and regional satellite-based NO_2 trend analysis. Section 3 describes the datasets used in this study and introduces the methodology applied for calculating the trends. Section 4 subsequently presents the results, including a full overview of the derived trends and statistics for all sites, a discussion of large-scale spatial patterns in trends, an analysis of a global average time series, a discussion of the impact of the time series extraction methodology, and finally a discussion of the relationship between NO_2 trends and population growth. Section 5 then provides a summary and conclusions.

2 Background

Spaceborne observations of NO_2 have been carried out since 1995 when the Global Ozone Monitoring Experiment (GOME) instrument was launched on the European ERS-1 platform. Since then, several studies have investigated temporal trends in tropospheric NO_2 provided by spaceborne platforms. Richter et al. (2005) were the first to study space-based NO_2 trends and provided a trend analysis based primarily on GOME NO_2 data over China. Later on, van der A et al. (2006) and van der A et al. (2008) combined data from the GOME and the SCIAMACHY instrument and provided a trend analysis focused on China and over the entire globe, respectively. A combination of GOME and SCIAMACHY data was also used by Ghude et al. (2009) for studying regional trends in tropospheric NO_2. Using a similar methodology, NO_2 trends over emission hotspots in India were further studied by Ghude et al. (2008). Summertime trends in European NO_x emissions were studied by Konovalov et al. (2008) using a combination of GOME, SCIAMACHY, and a continental-scale air quality model. The

ACPD
14, 24311–24348, 2014

methodology was later extended to study non-linear NO_2 and NO_x trends for several urban agglomerations in Europe and Asia, using method based on a probabilistic approach and artificial neural networks (Konovalov et al., 2010). The same combination of satellite instruments was further used by Kim et al. (2006) to quantify decreases in NO_x emissions over US power plants. Russell et al. (2012) studied the effect of emission control measures and the impact of the economic recession in the United States using OMI data. De Ruyter de Wildt et al. (2012) further investigated trends of tropospheric NO_2 over some of the major shipping lanes in the world.

Schneider and van der A (2012) made use of a homogeneous 9 year time series acquired by the SCIAMACHY instrument and provided the first single-sensor global trend analysis of NO_2, thus avoiding the merging of datasets with substantially different spatial resolution and possible inter-sensor calibration issues. They further analyzed trends over some of the major megacities but did not provide much detail on this issue. For this study we follow the approach suggested by Schneider and van der A (2012) and use data from the SCIAMACHY instrument, however in contrast to Schneider and van der A (2012) we use the full SCIAMACHY archive and an improved version of the satellite data product. The chosen approach has the advantage of providing very homogeneous time series and therefore highly reliable trends. Combining data from multiple instruments generally requires either resampling to a coarser-resolution grid in order to eliminate the impact of different spatial resolutions (van der A et al., 2006, 2008) or involves schemes for homogenizing the datasets using resolution correction factors (Konovalov et al., 2006; Hilboll et al., 2013) or empirical statistical approaches taking into account level-shift (Mieruch et al., 2008; Hilboll et al., 2013). Although significant progress has been made in techniques on combining data from multiple instruments (Hilboll et al., 2013), computing trends from homogeneous time series based on a single instrument still has the advantage that the computed trends are very likely to be real geophysical trends and are guaranteed not to be affected by different characteristics between instruments.

ACPD
14, 24311–24348, 2014

3 Data and methodology

The data and methodology used here are largely consistent with those used previously in Schneider and van der A (2012). However, there are a few important novel aspects to this work: (a) the primary focus of the study lies on large urban agglomerations (b) the length of the time series has now been expanded to include the entire available archive of SCIAMACHY data ranging from August 2002 to March 2012 (c) a new and improved version of the NO_2 retrieval algorithm (v2.3) (Boersma et al., 2004) has been used, and (d) compared to previous studies the list of large urban agglomerations has been significantly expanded and the resulting trends are studied in more detail.

3.1 Satellite data

Data from the SCIAMACHY instrument onboard the European Space Agency's Envisat platform was used in this study as it provides a homogeneous 10 year time series of global tropospheric NO_2 observations (Bovensmann et al., 1999; Gottwald et al., 2011). SCIAMACHY is a hyperspectral UV/VIS/NIR passive imaging grating spectrometer observing the wavelength range of 214–2386 nm. The entire archive of SCIAMACHY NO_2 data was used (see Fig. 1). The record starts in August 2002 and ends in early April 2012 due to the loss of communication with the Envisat platform. The SCIAMACHY data product of monthly mean tropospheric NO_2 that was used here was processed by KNMI using a combined retrieval/assimilation approach (Boersma et al., 2004) and acquired from the website of the Tropospheric Emission Monitoring Internet Service (http://temis.nl/).

The product is derived in a three step approach consisting of (a) Differential Optical Absorption Spectroscopy (DOAS) retrieval of the slant column, (b) a separation of the tropospheric and stratospheric contribution based on the TM4 chemical transport model (Dentener et al., 2003; Boersma et al., 2007), and (c) conversion of the slant column densities (SCD) into vertical column densities (VCD) using a calculated air mass factor (AMF). While the retrieval in general considers all cloud radiance fractions, the

ACPD
14, 24311–24348, 2014

monthly means are calculated only from data with cloud radiance fractions of less than 50 %. The NO_2 product is provided on a global grid of 0.25° by 0.25° spatial resolution. Version 2.3 of the product was used here. In addition to the major improvements to the retrieval algorithm introduced with version 2.0 (Boersma et al. (2011), and summarized in Schneider and van der A, 2012), version 2.3 further improved the algorithm by correcting some minor retrieval errors. Further details on the specific retrieval methodology can be found in Boersma et al. (2004), Boersma et al. (2007), and Boersma et al. (2011), as well as on the TEMIS website (www.temis.nl).

NO_2 retrievals from SCIAMACHY have been validated in numerous studies, e.g. by Heue et al. (2005) using Airbone Multi-Axis Differential Optical Absorption Spectroscopy observations, by Boersma et al. (2009) using in situ surface observations in Israel, and by Irie et al. (2012) using inter-comparison techniques with NO_2 products derived from other satellite instrument as well as MAX-DOAS observations in Japan and China. The latter showed that SCIAMACHY-based tropospheric NO_2 columns were accurate with a −5 % bias and standard deviation of ±14 %. The impact of topography on SCIAMACHY NO_2 retrievals was investigated by Schaub et al. (2007) who found errors of up to 40 % over very complex terrain. Blond et al. (2007) inter-compared SCIAMACHY-based NO_2 retrievals with in situ station observations over Europe and found biases of less than 5 and 20 % for annual and seasonal averages, respectively.

3.2 Site selection

The large urban agglomerations studied here were selected primarily based on population size as given by United Nations (2012b). All “true” megacities, i.e. cities with a population of greater than 10 million inhabitants, were included. In addition, most urban agglomerations with a population of more than 5 million as well as some special-interest sites with slightly less than 5 million inhabitants were also considered. Such special interest-sites were defined on a case by case basis primarily based on properties such as rapid population growth and/or known air quality issues, characteristics as

ACPD
14, 24311–24348, 2014

a hotspot in an otherwise unpolluted region, or in order to support balancing the spatial distribution of study sites globally.

Overall, 66 large urban agglomerations were identified for the analysis. Of those, seven were located in Africa, fifteen in East Asia, seven in Europe, ten in North America, two in Oceania, six in South America, nine in South Asia, four in South-East Asia, and five in West Asia. A full list of the studied sites including additional information about their exact location and their estimated population is given in Table 1.

3.3 Trend analysis

At each of the sites identified based on the methodology described in Sect. 3.2, time series of mean monthly tropospheric NO_2 were extracted from the full SCIAMACHY archive between August 2002 and March 2012. Subsequently a statistic model was fitted to the time series over each site. The monthly average NO_2 tropospheric column C_t at time t (in months) was modeled following Weatherhead et al. (1998) and Schneider and van der A (2012) as

$$C_t = \mu + S_t + \frac{1}{12}\omega t + R_t \quad (1)$$

where μ is a constant, S_t is a seasonal component, ω is a linear trend and R_t is the residual variability. The seasonal component S_t is modeled as

$$S_t = \sum_{j=1}^{4}\left[\beta_{1,j}\sin\left(\frac{2\pi jt}{12}\right) + \beta_{2,j}\cos\left(\frac{2\pi jt}{12}\right)\right] \quad (2)$$

where $\beta_{1,1}$ through $\beta_{2,4}$ are coefficients of the fit. The residual variability R_t is assumed to be autoregressive of order 1 and was modeled as

$$R_t = \phi R_{t-1} + \epsilon_t \quad (3)$$

where ϕ is the first order autocorrelation and ϵ is a random error component.

ACPD
14, 24311–24348, 2014

Based on the work by Tiao et al. (1990) and Weatherhead et al. (1998) and following the methdology described in Schneider and van der A (2012), the significance of the trend was calculated such that the trend ω is considered as significant with a 95 % confidence if

$$|\omega/\sigma_\omega| > t_\omega \tag{4}$$

where σ_ω is the uncertainty of the trend and t_ω is the value of the Student's t distribution for a significance level of $\alpha = 0.05$ and the degrees of freedom given for the time series (Santer et al., 2000).

The trend uncertainty σ_ω is computed following Weatherhead et al. (1998) and Schneider and van der A (2012) as

$$\sigma_\omega = \left[\frac{\sigma_r}{n^{3/2}}\sqrt{\frac{1+\phi}{1-\phi}}\right] \tag{5}$$

where σ_r is the standard deviation of the de-trended residuals, n is the number of years with available data, and ϕ is the first-order autocorrelation.

Relative trends ω_{rel} given in % per year are computed from the absolute trends ω_{abs} given in $\times 10^{15}$ molecules cm^{-2} yr^{-1} with respect to the long-term average tropospheric NO_2 column $\overline{\text{VCD}_{\text{trop}}}$ extracted at each individual grid cell as

$$\omega_{\text{rel}} = \frac{\omega_{\text{abs}}}{\overline{\text{VCD}_{\text{trop}}}} \cdot 100 \tag{6}$$

This approach of calculating the relative magnitude of the NO_2 trends differs from those taken by previous studies (e.g. van der A et al., 2006, 2008; Hilboll et al., 2013) in that it does not use a single reference year at the beginning of the time series and thus is less sensitive to potential outliers at the gridcell level for the reference year. However, it should be noted that the relative trends reported in this study are therefore not directly comparable to previous studies as they generally show values of lower magnitude.

ACPD
14, 24311–24348, 2014

3.4 Data on population growth

Among other factors, the emissions of nitrogen oxides are generally highly dependent on population density (Lamsal et al., 2013). For this reason, the relationship between temporal changes in tropospheric NO_2 and population growth of the urban agglomerations was studied. For this purpose, data on relative population growth by decade in the world's large urban agglomerations with 750 000 inhabitants or more was acquired from the United Nations' World Urbanization Prospects dataset (United Nations, 2012b). Data on population growth was available for the period 2000 to 2010 which agrees very closely with the study period of 2002 to 2012 used here and is thus considered to be suitable for comparison.

4 Results and discussion

4.1 Global trends

Figure 2 shows a global map of the computed trends in tropospheric NO_2 over all studied large urban agglomerations. The overarching spatial patterns visible in the map indicate large-scale decreasing NO_2 levels over all study sites in North America, Europe, Australia and Japan, whereas moderately to rapidly increasing trends can be observed throughout China, South Asia, as well as most of Africa and South America.

A total number of 66 large urban agglomerations were analyzed. Overall, a majority of the studied sites (44 out of 66) exhibited trends that are statistically significant at the 95 % level. In total, 34 sites exhibited increasing trends of tropospheric NO_2 throughout the study period, 24 of which were found to be statistically significant. A total of 32 sites showed decreasing levels of tropospheric NO_2 during the study period, of which 20 sites did so at statistically significant magnitudes. It should be noted that in this study we compute trends of tropospheric NO_2 concentrations, which differ from the actual emissions. Despite the short life time of NO_x, the NO_2 concentration field develops

ACPD
14, 24311–24348, 2014

a smooth spatial pattern roughly resembling a Gaussian distribution over the emission source, i.e. the city. However, the long-term trends will remain the same regardless of the spatial pattern in the concentration field resembling more a Gaussian or a point source.

Figure 3 shows histograms of absolute and relative trends in tropospheric NO_2 over all the large urban agglomerations studied. The majority of absolute trends falls into the range of -1×10^{15} to 0.5×10^{15} molecules cm^{-2} yr^{-1}, but a few urban agglomerations show even more rapidly decreasing or increasing trends. Most of the relative trends fall into the range between -5 and 6 % yr^{-1}, but several of the Asian sites exceed this range with values greater than 6 % yr^{-1}.

The overall extreme values in trends are compiled for clarity and given in Table 2. All of these trends are statistically significant at the 95 % level. The maximum value both in absolute and relative terms were found for megacities in Asia, whereas the most rapid absolute and relative decreases were both found for cities in the United States.

It should be noted that among the "true" megacities, i.e. urban agglomerations with a population of greater than 10 million inhabitants, the city of Dhaka in Bangladesh is the site with the most rapidly increasing relative trend with an increase in tropospheric NO_2 levels of 10.3 % yr^{-1} for the period studied here. This is consistent with the multi-instrument trend results reported by Hilboll et al. (2013), although the actual relative trend values differ due to the use of a different methodology for calculating the relative trends (using a single reference year in Hilboll et al. (2013) vs. the long-term mean in Schneider and van der A (2012) and this study).

Table 3 shows the absolute and relative trends derived from the entire 2002 to 2012 SCIAMACHY archive for all megacities and large urban agglomerations. For each site the estimated trend uncertainties are also included. The 6 sites with the most rapidly increasing tropospheric NO_2 levels in absolute terms and in fact all sites with absolute trends exceeding 1×10^{15} molecules cm^{-2} yr^{-1} all are located in China. In addition to Kabul, three more sites exceed relative trends of 10 % yr^{-1}, namely Nairobi, Dhaka, and Chongqing.

ACPD
14, 24311–24348, 2014

4.2 Temporal analysis

Figure 4 (top) shows the average monthly time series computed over all study sites. While the typical seasonal cycle for NO_2 is quite obvious in the monthly data, no clear linear trend is visible from that data. This is due to the fact that the time series represents an average over all worldwide megacities and large urban agglomerations with widely varying characteristics, including both rapidly increasing trends in Asia as well as decreasing NO_2 levels in North America and Europe.

In order to better highlight the overall signal contained in the global monthly time series, Fig. 4 (bottom) further shows the 12-month moving average of the deseasonalized monthly time series. The most obvious characteristic in this plot is a significant drop in concentrations throughout the year 2008, which then continuous at low levels throughout 2009 and 2010, after which the levels recover again slightly until 2011. This feature is most likely related to the worldwide financial crisis which started in 2008 and had a substantial impact on the global economy during this period. This result provides a global perspective to supplement previous studies that looked in detail at NO_2 concentrations as a proxy for the economic downturn over a single megacity (Vrekoussis et al., 2013) or provided regional studies about the same topic (Russell et al., 2012; Castellanos and Boersma, 2012; De Ruyter de Wildt et al., 2012).

In addition to the global time series given in Fig. 4, average time series were also studied at the regional level. Figure 5 shows the interannual variability of tropospheric NO_2 over all studied megacities and urban agglomerations, averaged by region. To facilitate an easier comparison between regions, the time series are given as averaged relative anomalies from the long-term mean at each site. The large-scale spatial patterns discussed previously are confirmed in this figure, with the urban agglomerations in Europe and North America exhibiting substantial decreases in NO_2, and the regions of South Asia, West Asia, and Africa showing rapid increases over the only 9 year period. North American agglomerations show a particularly drastic decrease in NO_2 after 2005, continuing until the end of the study period. This is likely related to emission

ACPD
14, 24311–24348, 2014

reduction measures which have been carried out during this period. In European agglomerations the NO_2 decrease appears to have stopped after 2008. The South Asia region shows the clearest increasing signal as the urban agglomerations located in this area all exhibit positive trends. The averaged time series for East Asia and South America do not show a clear signal because the regions contain agglomerations with both increasing and decreasing NO_2 levels.

4.3 Impact of time series extraction methodology

The methodology by which the time series are extracted from the satellite data can to some extent affect the magnitude of the trends, depending on the spatial homogeneity of the trends patterns in the surroundings of each urban agglomeration. In order to study this, time series were extracted from the satellite data using two approaches. The first one only used the grid cell in which the center of the urban agglomeration was located. The second approach used the average value of a 3×3 grid cell array centered on the same location.

Figure 6 illustrates the effect of the size of the averaging region on the resulting absolute and relative trends when the time series are extracted either from a single grid cell (here denoted as $\omega_{\mathrm{abs}(1\times1)}$ and $\omega_{\mathrm{rel}(1\times1)}$), or as the average of a 3×3 grid cell array centered over the study site, here denoted as $\omega_{\mathrm{abs}(3\times3)}$ and $\omega_{\mathrm{rel}(3\times3)}$.

The mean difference between the absolute trends, calculated as $\omega_{\mathrm{abs}(1\times1)} - \omega_{\mathrm{abs}(3\times3)}$, from time series derived from a single grid vs. a 3×3 grid cell array was found to be 0.013×10^{15} molecules $\mathrm{cm}^{-2}\,\mathrm{yr}^{-1}$ with a standard deviation of 0.16×10^{15} molecules $\mathrm{cm}^{-2}\,\mathrm{yr}^{-1}$ and an root mean squared error (RMSE) of 0.16×10^{15} molecules $\mathrm{cm}^{-2}\,\mathrm{yr}^{-1}$. The largest deviation in absolute trends was found for Chengdu, China, with a difference of 0.5×10^{15} molecules $\mathrm{cm}^{-2}\,\mathrm{yr}^{-1}$. This is likely related to the specific orography of the region around Chengdu with high mountains surrounding the city to the South, West, and North. As for deviations in relative trends, calculated as $\omega_{\mathrm{rel}(1\times1)} - \omega_{\mathrm{rel}(3\times3)}$, the mean difference was found to be $0.25\,\%\,\mathrm{yr}^{-1}$ with

ACPD
14, 24311–24348, 2014

a standard deviation of 1.09 % yr^{-1} and an RMSE of 1.1 % yr^{-1}. The largest deviation in terms of relative trends was observed for the city of Lagos, Nigeria, with a value of 4.18 % yr^{-1}.

The results indicate that the two approaches are quite comparable and mostly differ by values that are negligible as compared to the overall magnitude of the trends and their estimated uncertainties. However, for a few cases, such as for example the city of Lagos, the trend difference between the two extraction approaches reaches values that exceed 50 % of the actual trend value and thus can have a significant impact on the results. Obviously, the differences observed here are to a large extent due to variability in the spatial extent of the urban agglomerations and not in all cases a 3 × 3 grid cell average is warranted Since columns rather than emissions are studied here, the spatial patterns over a NO_x source such as a megacity will mostly appear spatially smoothed, which limits the effect of spatial gradients. As such, the spatial variability and the area over which the trends are computed will generally only play a significant role for agglomerations with a very large spatial extent as for example the greater Los Angeles area, which covers substantially more than 9 grid cells.

Therefore, while the 3 × 3 grid cell array approach has the advantage of providing more valid monthly mean values and thus time series which result in a slightly better model fit, it was decided here to use the single grid cell approach for extracting the time series as it ensures that all sites are well represented in the time series, independent of the spatial shape and size of the city. For agglomerations with a very large spatial extent, such as Los Angeles, future work could explore the option of calculating the trends over the entire area covered by each site, for example as given by polygon outlines.

4.4 NO_2 trends and population growth

NO_2 concentrations are generally closely linked to population density (Lamsal et al., 2013). For this reason, the worldwide trends obtained from SCIAMACHY for the studied

ACPD
14, 24311–24348, 2014

large urban agglomerations were compared with data on population growth at the same sites.

Figure 7 shows the relationship between population growth for the period 2000 to 2010 and satellite-derived trends in tropospheric NO_2 for the period 2002 to 2012, classified by region. The results show distinctly different behavior for each region. A linear relationship between NO_2 trend and population growth can be seen for large urban agglomerations in Europe and South Asia.

In Europe the relationship roughly follows the regression equation $\omega_{rel} = -3.8 + 1.6 \cdot PG$, where ω_{rel} is the SCIAMACHY-derived relative trend in tropospheric NO_2 concentration in % yr^{-1} and PG is the population growth over the 2000 through 2010 period given in %. This relationship has an R^2 value of 0.74.

Similarly, in South Asia the relationship roughly follows the regression equation $\omega_{rel} = -1.7 + 2.1 \cdot PG$ with an R^2 value of 0.72. It should be noted, however, that both relationships are based on a relatively small sample size of $N = 7$ and $N = 10$ for Europe and South Asia, respectively.

In other regions besides Europe and South Asia, no obvious linear relationships are visible in Fig. 7, although distinct patterns clearly emerge. For East Asia, a clear division between Chinese and primarily Japanese/Korean agglomerations (with the exception of Hong Kong) is visible, with the former exhibiting both strong population growth and rapid increases in tropospheric NO_2, whereas the latter show very weak population growth (or even -loss) and decreases in tropospheric NO_2 between 0 and $-5\,\%\,yr^{-1}$. A special case are the two Chinese megacities of Guanghzou and Shenzhen which, despite having strong population growth, exhibit decreasing levels of NO_2, most likely due to politically motivated emission reduction measures in this area.

Only 5 sites were available in West Asia and no clear pattern or relationship can be inferred. Baghdad has a surprisingly rapid increase in tropospheric NO_2 levels of $9\,\%\,yr^{-1}$ given its population growth of only around 1 %.

Megacities and large urban agglomerations in North and South America clearly fall into one of two main clusters. North American agglomerations exhibit moderate

ACPD
14, 24311–24348, 2014

population growth between 0 and 4 % for the 2000 to 2010 period, however they all clearly show NO_2 decreases between −5 and −10 % yr^{-1}. The exception here is Mexico City, which only exhibits very minor NO_2 decreases. The other cluster is formed by South American agglomerations which exhibit mostly similar rates of population growth but, with the exception of Bogota, show constant or increasing tropospheric NO_2 levels.

Finally, African megacities and agglomerations do not indicate a strong relationship or other patterns. With most sites except Cairo exhibiting population growth rates greater than 2 % for 2000–2010, Johannesburg is the only African site with decreasing tropospheric NO_2 levels. All other sites exhibit growth in NO_2 concentrations which in the case of Nairobi reach very high levels of over 13 % yr^{-1}.

5 Conclusions

Megacities and other large urban agglomerations are major hotspots for air pollution. Given the substantial global population growth and the strong tendency towards urbanization, this problem will be exacerbated in future decades. Here we present an overview of recent changes and trends in tropospheric NO_2 concentrations over 66 of the largest urban agglomerations worldwide. The trends were derived by fitting a statistical model including a linear trend and a seasonal component to time series extracted from the full SCIAMACHY satellite data archive for the period August 2002 to March 2012.

Overall, 45 sites showed statistically significant trends at the 95 % level. Of those, 34 sites exhibited increasing trends of tropospheric NO_2 throughout the study period, 24 of which were found to be statistically significant. In addition, 32 sites showed decreasing levels of tropospheric NO_2 during the study period, of which 20 sites did so at statistically significant magnitudes. The most extreme increasing absolute and relative values in trends during the study period were found for two Asian sites (Tianjin in China and Kabul in Afghanistan, respectively), whereas the most rapidly decreasing absolute

ACPD
14, 24311–24348, 2014

and relative trends were observed for two sites in North America (Los Angeles and Boston, respectively).

Spatial patterns in worldwide trends for megacities and large urban agglomerations were studied. Similarly to previous studies investigating global tropospheric NO_2 trends (van der A et al., 2008; Schneider and van der A, 2012; Hilboll et al., 2013), the characteristics patterns for trends over urban agglomerations include a spatially homogeneous reduction in concentrations over both Europe and North America on the level of around $-5\,\%\,yr^{-1}$, and moderately to rapidly increasing concentrations over large parts of Asia as well as Africa and South America, reaching relative trend magnitudes as high as $15\,\%\,yr^{-1}$.

In addition to spatial patterns, the time series over the urban agglomerations were studied both at the global and regional level. At the global level no strong overall trends were observed but a signal of the 2008/2009 economical crisis was identified. The analysis of average time series at the regional level confirmed the overall patterns found in the spatial analysis. Finally, the relationship between the satellite-derived NO_2 trends over urban agglomerations and urban population growth was investigated. Clear linear relationships were found for Europe and South Asia, but other regions did not indicate such relationships, although characteristic clusters distinguishing sites in developing vs. developed countries did emerge.

An important next step will be the direct validation of satellite-derived trends in tropospheric NO_2. There are now several stations worldwide providing observations from Multi-Axis Differential Optical Absorption Spectroscopy (MAX-DOAS) instruments (Hönninger et al., 2004; Irie et al., 2012; Kanaya et al., 2014; Hendrick et al., 2014), providing highly accurate measurements of tropospheric columns of various trace gases. Some of these stations now provide time series of 5 years and more, thus allowing for a direct comparison of satellite-derived trends with trends obtained from a reliable reference source. Such a direct validation will add value to NO_2 trends computed from the various satellite products as it will provide a realistic estimate of the uncertainty involved in such analyses.

ACPD
14, 24311–24348, 2014

Acknowledgements. This work has been partially supported by the MACC-II project funded by the European Union under the Seventh Framework Programme (FP7 THEME [SPA.2011.1.5-02]) under grant agreement n. 283576. Further funding was provided by the Norwegian Space Centre within the SatMonAir-I and SatMonAir-II projects. We gratefully acknowledge the free use of tropospheric NO_2 column data from the SCIAMACHY sensor provided by www.temis.nl.

References

Baklanov, A., Lawrence, M., Pandis, S., Mahura, A., Finardi, S., Moussiopoulos, N., Beekmann, M., Laj, P., Gomes, L., Jaffrezo, J.-L., Borbon, A., Coll, I., Gros, V., Sciare, J., Kukkonen, J., Galmarini, S., Giorgi, F., Grimmond, S., Esau, I., Stohl, A., Denby, B., Wagner, T., Butler, T., Baltensperger, U., Builtjes, P., van den Hout, D., van der Gon, H. D., Collins, B., Schluenzen, H., Kulmala, M., Zilitinkevich, S., Sokhi, R., Friedrich, R., Theloke, J., Kummer, U., Jalkinen, L., Halenka, T., Wiedensholer, A., Pyle, J., and Rossow, W. B.: MEGAPOLI: concept of multi-scale modelling of megacity impact on air quality and climate, Adv. Sci. Res., 4, 115–120, doi:10.5194/asr-4-115-2010, 2010. 24313

Blond, N., Boersma, K. F., Eskes, H. J., van der A, R. J., Van Roozendael, M., De Smedt, I., Bergametti, G., and Vautard, R.: Intercomparison of SCIAMACHY nitrogen dioxide observations, in situ measurements and air quality modeling results over Western Europe, J. Geophys. Res., 112, 1–20, doi:10.1029/2006JD007277, 2007. 24317

Boersma, K. F., Eskes, H. F., and Brinksma, E. J.: Error analysis for tropospheric NO_2 retrieval from space, J. Geophys. Res., 109, D04311, doi:10.1029/2003JD003962, 2004. 24316, 24317

Boersma, K. F., Eskes, H. J., Veefkind, J. P., Brinksma, E. J., van der A, R. J., Sneep, M., van den Oord, G. H. J., Levelt, P. F., Stammes, P., Gleason, J. F., and Bucsela, E. J.: Near-real time retrieval of tropospheric NO_2 from OMI, Atmos. Chem. Phys., 7, 2103–2118, doi:10.5194/acp-7-2103-2007, 2007. 24316, 24317

Boersma, K. F., Jacob, D. J., Trainic, M., Rudich, Y., DeSmedt, I., Dirksen, R., and Eskes, H. J.: Validation of urban NO_2 concentrations and their diurnal and seasonal variations observed from the SCIAMACHY and OMI sensors using in situ surface measurements in Israeli cities, Atmos. Chem. Phys., 9, 3867–3879, doi:10.5194/acp-9-3867-2009, 2009. 24317

ACPD
14, 24311–24348, 2014

Boersma, K. F., Eskes, H. J., Dirksen, R. J., van der A, R. J., Veefkind, J. P., Stammes, P., Huijnen, V., Kleipool, Q. L., Sneep, M., Claas, J., Leitão, J., Richter, A., Zhou, Y., and Brunner, D.: An improved tropospheric NO_2 column retrieval algorithm for the Ozone Monitoring Instrument, Atmos. Meas. Tech., 4, 1905–1928, doi:10.5194/amt-4-1905-2011, 2011. 24317

Bovensmann, H., Burrows, J. P., Buchwitz, M., Frerick, J., Noël, S., Rozanov, V. V., Chance, K. V., and Goede, A. P. H.: SCIAMACHY: Mission Objectives and Measurement Modes, J. Atmos. Sci., 56, 127–150, doi:10.1175/1520-0469(1999)056<0127:SMOAMM>2.0.CO;2, 1999. 24316

Cassiani, M., Stohl, A., and Eckhardt, S.: The dispersion characteristics of air pollution from the world's megacities, Atmos. Chem. Phys., 13, 9975–9996, doi:10.5194/acp-13-9975-2013, 2013. 24313

Castellanos, P. and Boersma, K. F.: Reductions in nitrogen oxides over Europe driven by environmental policy and economic recession, Scientific Reports, 2, 265, doi:10.1038/srep00265, 2012. 24322

Chan, C. K. and Yao, X.: Air pollution in mega cities in China, Atmos. Environ., 42, 1–42, doi:10.1016/j.atmosenv.2007.09.003, 2008. 24313

De Ruyter de Wildt, M., Eskes, H., and Boersma, K. F.: The global economic cycle and satellite-derived NO_2 trends over shipping lanes, Geophys. Res. Lett., 39, 2–7, doi:10.1029/2011GL049541, 2012. 24315, 24322

Dentener, F., van Weele, M., Krol, M., Houweling, S., and van Velthoven, P.: Trends and inter-annual variability of methane emissions derived from 1979-1993 global CTM simulations, Atmos. Chem. Phys., 3, 73–88, doi:10.5194/acp-3-73-2003, 2003. 24316

Fenger, J.: Urban air quality, Atmos. Environ., 33, 4877–4900, doi:10.1016/S1352-2310(99)00290-3, 1999. 24313

Flemming, J., Inness, A., Flentje, H., Huijnen, V., Moinat, P., Schultz, M. G., and Stein, O.: Coupling global chemistry transport models to ECMWF's integrated forecast system, Geosci. Model Dev., 2, 253–265, doi:10.5194/gmd-2-253-2009, 2009. 24313

Ghude, S. D., Fadnavis, S., Beig, G., Polade, S. D., and van der A, R. J.: Detection of surface emission hot spots, trends, and seasonal cycle from satellite-retrieved NO_2 over India, J. Geophys. Res., 113, 1–13, doi:10.1029/2007JD009615, 2008. 24314

Ghude, S. D., Van der A, R. J., Beig, G., Fadnavis, S., and Polade, S. D.: Satellite derived trends in NO_2 over the major global hotspot regions during the past decade and their

ACPD
14, 24311–24348, 2014

inter-comparison, Environ. Pollut., 157, 1873–1878, doi:10.1016/j.envpol.2009.01.013, 2009. 24314
Gottwald, M., Bovensmann, H., Lichtenberg, G., Noel, S., Bargen, A. von, Slijkhuis, S., Piters, A., Hoogeveen, R., Savigny, C. von, Buchwitz, M., Kokhanovsky, A., Richter, A., Rozanov, A., Holzer-Popp, T., Bramstedt, K., Lambert, J.-C., Skupin, J., Wittrock, F., Schrijver, H., and Burrows, J. P.: SCIAMACHY – Exploring the Changing Earth's Atmosphere, Springer, Dordrecht, the Netherlands, 2011. 24316
Gurjar, B., Butler, T., Lawrence, M., and Lelieveld, J.: Evaluation of emissions and air quality in megacities, Atmos. Environ., 42, 1593–1606, doi:10.1016/j.atmosenv.2007.10.048, 2008. 24313
Gurjar, B., Jain, A., Sharma, A., Agarwal, A., Gupta, P., Nagpure, A. S., and Lelieveld, J.: Human health risks in megacities due to air pollution, Atmos. Environ., 44, 4606–4613, doi:10.1016/j.atmosenv.2010.08.011, 2010. 24313
Hendrick, F., Müller, J.-F., Clémer, K., Wang, P., De Mazière, M., Fayt, C., Gielen, C., Hermans, C., Ma, J. Z., Pinardi, G., Stavrakou, T., Vlemmix, T., and Van Roozendael, M.: Four years of ground-based MAX-DOAS observations of HONO and NO_2 in the Beijing area, Atmos. Chem. Phys., 14, 765–781, doi:10.5194/acp-14-765-2014, 2014. 24327
Heue, K.-P., Richter, A., Bruns, M., Burrows, J. P., v. Friedeburg, C., Platt, U., Pundt, I., Wang, P., and Wagner, T.: Validation of SCIAMACHY tropospheric NO_2-columns with AMAXDOAS measurements, Atmos. Chem. Phys., 5, 1039–1051, doi:10.5194/acp-5-1039-2005, 2005. 24317
Hilboll, A., Richter, A., and Burrows, J. P.: Long-term changes of tropospheric NO_2 over megacities derived from multiple satellite instruments, Atmos. Chem. Phys., 13, 4145–4169, doi:10.5194/acp-13-4145-2013, 2013. 24313, 24315, 24319, 24321, 24327
Hönninger, G., von Friedeburg, C., and Platt, U.: Multi axis differential optical absorption spectroscopy (MAX-DOAS), Atmos. Chem. Phys., 4, 231–254, doi:10.5194/acp-4-231-2004, 2004. 24327
Inness, A., Baier, F., Benedetti, A., Bouarar, I., Chabrillat, S., Clark, H., Clerbaux, C., Coheur, P., Engelen, R. J., Errera, Q., Flemming, J., George, M., Granier, C., Hadji-Lazaro, J., Huijnen, V., Hurtmans, D., Jones, L., Kaiser, J. W., Kapsomenakis, J., Lefever, K., Leitão, J., Razinger, M., Richter, A., Schultz, M. G., Simmons, A. J., Suttie, M., Stein, O., Thépaut, J.-N., Thouret, V., Vrekoussis, M., Zerefos, C., and the MACC team: The MACC reanalysis: an 8 yr

ACPD
14, 24311–24348, 2014

data set of atmospheric composition, Atmos. Chem. Phys., 13, 4073–4109, doi:10.5194/acp-13-4073-2013, 2013. 24313

Irie, H., Boersma, K. F., Kanaya, Y., Takashima, H., Pan, X., and Wang, Z. F.: Quantitative bias estimates for tropospheric NO_2 columns retrieved from SCIAMACHY, OMI, and GOME-2 using a common standard for East Asia, Atmos. Meas. Tech., 5, 2403–2411, doi:10.5194/amt-5-2403-2012, 2012. 24317, 24327

Kanakidou, M., Mihalopoulos, N., Kindap, T., Im, U., Vrekoussis, M., Gerasopoulos, E., Dermitzaki, E., Unal, A., Koçak, M., Markakis, K., Melas, D., Kouvarakis, G., Youssef, A. F., Richter, A., Hatzianastassiou, N., Hilboll, A., Ebojie, F., Wittrock, F., von Savigny, C., Burrows, J. P., Ladstaetter-Weissenmayer, A., and Moubasher, H.: Megacities as hot spots of air pollution in the East Mediterranean, Atmos. Environ., 45, 1223–1235, doi:10.1016/j.atmosenv.2010.11.048, 2011. 24313

Kanaya, Y., Irie, H., Takashima, H., Iwabuchi, H., Akimoto, H., Sudo, K., Gu, M., Chong, J., Kim, Y. J., Lee, H., Li, A., Si, F., Xu, J., Xie, P.-H., Liu, W.-Q., Dzhola, A., Postylyakov, O., Ivanov, V., Grechko, E., Terpugova, S., and Panchenko, M.: Long-term MAX-DOAS network observations of NO_2 in Russia and Asia (MADRAS) during the period 2007–2012: instrumentation, elucidation of climatology, and comparisons with OMI satellite observations and global model simulations, Atmos. Chem. Phys., 14, 7909–7927, doi:10.5194/acp-14-7909-2014, 2014. 24327

Kim, S.-W., Heckel, A., McKeen, S. A., Frost, G. J., Hsie, E.-Y., Trainer, M. K., Richter, A., Burrows, J. P., Peckham, S. E., and Grell, G. A.: Satellite-observed U. S. power plant NO_x emission reductions and their impact on air quality, Geophys. Res. Lett., 33, 1–5, doi:10.1029/2006GL027749, 2006. 24315

Konovalov, I. B., Beekmann, M., Richter, A., and Burrows, J. P.: Inverse modelling of the spatial distribution of NO_x emissions on a continental scale using satellite data, Atmos. Chem. Phys., 6, 1747–1770, doi:10.5194/acp-6-1747-2006, 2006. 24315

Konovalov, I. B., Beekmann, M., Burrows, J. P., and Richter, A.: Satellite measurement based estimates of decadal changes in European nitrogen oxides emissions, Atmos. Chem. Phys., 8, 2623–2641, doi:10.5194/acp-8-2623-2008, 2008. 24314

Konovalov, I. B., Beekmann, M., Richter, A., Burrows, J. P., and Hilboll, A.: Multi-annual changes of NO_x emissions in megacity regions: nonlinear trend analysis of satellite measurement based estimates, Atmos. Chem. Phys., 10, 8481–8498, doi:10.5194/acp-10-8481-2010, 2010. 24315

ACPD
14, 24311–24348, 2014

Lahoz, W. A. and Schneider, P.: Data assimilation: making sense of Earth Observation, Frontiers in Environmental Science, 2, 1–28, doi:10.3389/fenvs.2014.00016, 2014. 24313
Lamsal, L. N., Martin, R. V., Parrish, D. D., and Krotkov, N. A.: Scaling relationship for NO_2 pollution and urban population size: a satellite perspective, Environ. Sci. Technol., 47, 7855–7861, doi:10.1021/es400744g, 2013. 24313, 24320, 24324
Mage, D., Ozolins, G., Peterson, P., Webster, A., Orthofer, R., Vandeweerd, V., and Gwynne, M.: Urban air pollution in megacities of the world, Atmos. Environ., 30, 681–686, doi:10.1016/1352-2310(95)00219-7, 1996. 24313
Mayer, H.: Air pollution in cities, Atmos. Environ., 33, 4029–4037, doi:10.1016/S1352-2310(99)00144-2, 1999. 24313
Mieruch, S., Noël, S., Bovensmann, H., and Burrows, J. P.: Analysis of global water vapour trends from satellite measurements in the visible spectral range, Atmos. Chem. Phys., 8, 491–504, doi:10.5194/acp-8-491-2008, 2008. 24315
Molina, L. T., Molina, M. J., Slott, R. S., Kolb, C. E., Gbor, P. K., Meng, F., Singh, R. B., Galvez, O., Sloan, J. J., Anderson, W. P., Tang, X., Hu, M., Xie, S., Shao, M., Zhu, T., Zhang, Y., Gurjar, B. R., Artaxo, P. E., Oyola, P., Gramsch, E., Hidalgo, D., and Gertler, A. W.: Air quality in selected megacities, J. Air Waste Manage., 54, 1–73, doi:10.1080/10473289.2004.10471015, 2004. 24313
Molina, M. J. and Molina, L. T.: Megacities and atmospheric pollution, J. Air Waste Manage., 54, 644–680, doi:10.1080/10473289.2004.10470936, 2004. 24313
Monks, P., Granier, C., Fuzzi, S., Stohl, A., Williams, M., Akimoto, H., Amann, M., Baklanov, A., Baltensperger, U., Bey, I., Blake, N., Blake, R., Carslaw, K., Cooper, O., Dentener, F., Fowler, D., Fragkou, E., Frost, G., Generoso, S., Ginoux, P., Grewe, V., Guenther, A., Hansson, H., Henne, S., Hjorth, J., Hofzumahaus, A., Huntrieser, H., Isaksen, I., Jenkin, M., Kaiser, J., Kanakidou, M., Klimont, Z., Kulmala, M., Laj, P., Lawrence, M., Lee, J., Liousse, C., Maione, M., McFiggans, G., Metzger, A., Mieville, A., Moussiopoulos, N., Orlando, J., O'Dowd, C., Palmer, P., Parrish, D., Petzold, A., Platt, U., Pöschl, U., Prévôt, A., Reeves, C., Reimann, S., Rudich, Y., Sellegri, K., Steinbrecher, R., Simpson, D., ten Brink, H., Theloke, J., van der Werf, G., Vautard, R., Vestreng, V., Vlachokostas, C., and von Glasow, R.: Atmospheric composition change – global and regional air quality, Atmos. Environ., 43, 5268–5350, doi:10.1016/j.atmosenv.2009.08.021, 2009. 24313

ACPD
14, 24311–24348, 2014

Parrish, D. D., Singh, H. B., Molina, L., and Madronich, S.: Air quality progress in North American megacities: a review, Atmos. Environ., 45, 7015–7025, doi:10.1016/j.atmosenv.2011.09.039, 2011. 24313

Richter, A., Burrows, J. P., Nüss, H., Granier, C., and Niemeier, U.: Increase in tropospheric nitrogen dioxide over China observed from space, Nature, 437, 129–32, doi:10.1038/nature04092, 2005. 24313, 24314

Russell, A. R., Valin, L. C., and Cohen, R. C.: Trends in OMI NO_2 observations over the United States: effects of emission control technology and the economic recession, Atmos. Chem. Phys., 12, 12197–12209, doi:10.5194/acp-12-12197-2012, 2012. 24315, 24322

Santer, B., Wigley, T., Boyle, J., Gaffen, D., Hnilo, J., Nychka, D., Parker, D., and Taylor, K.: Statistical significance of trends and trend differences in layer-average atmospheric temperature time series, J. Geophys. Res., 105, 7337–7356, 2000. 24319

Schaub, D., Brunner, D., Boersma, K. F., Keller, J., Folini, D., Buchmann, B., Berresheim, H., and Staehelin, J.: SCIAMACHY tropospheric NO_2 over Switzerland: estimates of NO_x lifetimes and impact of the complex Alpine topography on the retrieval, Atmos. Chem. Phys., 7, 5971–5987, doi:10.5194/acp-7-5971-2007, 2007. 24317

Schneider, P. and van der A, R. J.: A global single-sensor analysis of 2002–2011 tropospheric nitrogen dioxide trends observed from space, J. Geophys. Res., 117, 1–17, doi:10.1029/2012JD017571, 2012. 24313, 24315, 24316, 24317, 24318, 24319, 24321, 24327

Tiao, G., Reinsel, G. C., Daming, X., Pedrick, J. H., Xiaodong, Z., Miller, A. J., DeLuisi, J. J., Mateer, C. L., and Wuebbles, D. J.: Effects of autocorrelation and temporal sampling schemes on estimates of trend and spatial correlation, J. Geophys. Res., 95, 20507–20517, 1990. 24319

United Nations: World Urbanization Prospects The 2011 Revision – Highlights, Tech. rep., United Nations – Department of Economic and Social Affairs – Population Division, New York, NY, 2012a. 24312

United Nations: World Urbanization Prospects: The 2011 Revision – CD-ROM Edition, available at: http://esa.un.org/unpd/wpp/index.htm (last access: 2 June 2014), 2012b. 24317, 24320, 24335

van der A, R. J., Peters, D. H. M. U., Eskes, H., Boersma, K. F., Van Roozendael, M., De Smedt, I., and Kelder, H. M.: Detection of the trend and seasonal variation in tropospheric

ACPD
14, 24311–24348, 2014

NO_2 over China, J. Geophys. Res., 111, 1–10, doi:10.1029/2005JD006594, 2006. 24314, 24315, 24319

van der A, R. J., Eskes, H. J., Boersma, K. F., van Noije, T. P. C., Van Roozendael, M., De Smedt, I., Peters, D. H. M. U., and Meijer, E. W.: Trends, seasonal variability and dominant NO_x source derived from a ten year record of NO_2 measured from space, J. Geophys. Res., 113, 1–12, doi:10.1029/2007JD009021, 2008. 24313, 24314, 24315, 24319, 24327

Vrekoussis, M., Richter, A., Hilboll, A., Burrows, J. P., Gerasopoulos, E., Lelieveld, J., Barrie, L., Zerefos, C., and Mihalopoulos, N.: Economic crisis detected from space: air quality observations over Athens/Greece, Geophys. Res. Lett., 40, 458–463, doi:10.1002/grl.50118, 2013. 24322

Weatherhead, E., Reinsel, G., Tiao, G., Meng, X., Choi, D., Cheang, W., Keller, T., DeLuisi, J., Wuebbles, D., Kerr, J., and Others: Factors affecting the detection of trends: statistical considerations and applications to environmental data, J. Geophys. Res.-Atmos., 103, 17149–17161, 1998. 24318, 24319

Zhu, T., Melamed, M. L., Parrish, D., Gauss, M., Gallardo Klenner, L., Lawrence, M., Konare, A., and Liousse, C.: Impacts of Megacities on Air Pollution and Climate, Tech. Rep. 205, WMO/IGAC, Geneva, Switzerland, 2012. 24312

ACPD
14, 24311–24348, 2014

Table 1. Metadata of the selected megacities and other large urban agglomerations. A total of 66 sites were selected based on the criteria listed in Sect. 3.2. The given latitude and longitude values indicate the location at which the time series was extracted from the SCIAMACHY dataset. The data on estimated population was taken from United Nations (2012b).

City Name	Country	Lat. [° N]	Lon. [° E]	Pop. [mill.]
Algiers	Algeria	36.76	3.04	3.4
Athens	Greece	37.98	23.73	3.6
Atlanta	USA	33.76	−84.39	5.4
Baghdad	Iraq	33.32	44.40	6.4
Bangalore	India	12.97	77.60	9.5
Bangkok	Thailand	13.72	100.54	14.3
Beijing	China	39.91	116.37	16.9
Bogota	Colombia	4.65	−74.10	9.2
Boston	USA	42.37	−71.07	7.2
Buenos Aires	Argentina	−34.62	−58.46	14.5
Cairo	Egypt	30.04	31.24	16.0
Chengdu	China	30.66	104.06	6.4
Chicago	USA	41.88	−87.67	9.8
Chongqing	China	29.56	106.55	6.4
Damascus	Syria	33.51	36.30	3.5
Delhi	India	28.63	77.22	23.7
Dhaka	Bangladesh	23.74	90.40	16.0
Guangzhou	China	23.13	113.24	26.4
Ho Chi Minh City	Vietnam	10.78	106.66	8.1
Hong Kong	China	22.32	114.18	7.2
Houston	USA	29.76	−95.37	5.9
Hyderabad	India	17.39	78.48	8.5
Istanbul	Turkey	41.01	28.97	13.6
Jakarta	Indonesia	−6.22	106.85	26.0
Jeddah	Saudi Arabia	21.53	39.20	3.9
Johannesburg	South Africa	−26.20	28.04	8.5

ACPD
14, 24311–24348, 2014

Table 1. Continued.

City Name	Country	Lat. [° N]	Lon. [° E]	Pop. [mill.]
Kabul	Afghanistan	34.53	69.17	3.5
Karachi	Pakistan	24.88	67.04	22.3
Khartoum	Sudan	15.55	32.53	5.2
Kinshasa	Congo	−4.34	15.31	9.8
Kolkata	India	22.57	88.36	15.9
Lagos	Nigeria	6.51	3.35	13.0
Lahore	Pakistan	31.51	74.34	9.4
Lima	Peru	−12.05	−77.04	9.6
London	Great Britain	51.51	−0.11	13.3
Los Angeles	USA	33.92	−118.08	17.1
Madras	India	13.07	80.22	9.5
Manila	Philippines	14.61	121.02	21.9
Melbourne	Australia	−37.80	145.05	4.2
Mexico City	Mexico	19.42	−99.13	23.6
Moscow	Russia	55.75	37.62	16.3
Mumbai	India	19.08	72.88	21.2
Nagoya	Japan	35.19	136.85	8.5
Nairobi	Kenya	−1.29	36.83	4.7
New York	USA	40.76	−73.97	21.6
Osaka	Japan	34.65	135.51	16.8
Paris	France	48.86	2.35	10.6
Philadelphia	USA	39.96	−75.16	7.3
Po Valley	Italy	45.47	9.19	24.3
Rhein-Ruhr	Germany	51.49	7.08	4.6
Rio de Janeiro	Brazil	−22.85	−43.32	12.8
Riyadh	Saudi Arabia	24.69	46.73	6.1

ACPD
14, 24311–24348, 2014

Table 1. Continued.

City Name	Country	Lat. [° N]	Lon. [° E]	Pop. [mill.]
San Francisco	USA	37.75	−122.43	7.2
Santiago	Chile	−33.46	−70.64	6.3
Sao Paulo	Brazil	−23.55	−46.64	21.4
Seoul	Korea (South)	37.54	126.97	25.6
Shanghai	China	31.23	121.48	26.0
Shenyang	China	41.81	123.43	7.3
Shenzhen	China	22.58	114.05	10.1
Sydney	Australia	−33.91	151.06	4.7
Taipei	Taiwan	25.04	121.51	9.0
Tehran	Iran	35.70	51.41	13.8
Tianjin	China	39.14	117.20	10.1
Tokyo	Japan	35.70	139.76	34.7
Washington	USA	38.90	−77.02	8.1
Wuhan	China	30.56	114.32	9.3

ACPD
14, 24311–24348, 2014

Table 2. Extreme values among the studied large urban agglomerations, both in terms of absolute and relative trends. All of the listed trends are statistically significant at the $p < 0.05$ level.

	Absolute Trends	Relative Trends
Largest positive	Tianjin, China $2.83(\pm 0.48) \times 10^{15}$ molecules cm^{-2} yr^{-1}	Kabul, Afghanistan $14.3(\pm 2.2)$ % yr^{-1}
Largest negative	Los Angeles, USA $-1.66(\pm 0.31) \times 10^{15}$ molecules cm^{-2} yr^{-1}	Boston, USA $-9.0(\pm 3.0)$ % yr^{-1}

ACPD
14, 24311–24348, 2014

Table 3. Trend analysis results for all studied large urban agglomerations. The absolute trends and their uncertainty are given in units of $\times 10^{15}$ molecules cm^{-2} yr^{-1} and the relative trends and their uncertainty are given in % yr^{-1}. The trends shown here were computed using time series extracted from a single grid cell located over the center of each agglomeration. The relative trends were computed with respect to the long term mean of the time series over a given grid cell. Trends that were found to be statistically significant at the $p < 0.05$ level are marked in bold.

City	N	Absolute Trend	Relative Trend
Algiers	115	0.096 ± 0.066	2.4 ± 1.7
Athens	114	**−0.213 ± 0.081**	**−3.6 ± 1.4**
Atlanta	108	**−0.449 ± 0.111**	**−5.4 ± 1.3**
Baghdad	115	**0.600 ± 0.085**	**8.5 ± 1.2**
Bangalore	87	**0.188 ± 0.058**	**6.1 ± 1.9**
Bangkok	116	0.203 ± 0.163	1.9 ± 1.6
Beijing	110	0.152 ± 0.552	0.4 ± 1.3
Bogota	38	**−0.250 ± 0.091**	**−3.4 ± 1.2**
Boston	108	**−0.828 ± 0.281**	**−9.0 ± 3.0**
Buenos Aires	113	**0.249 ± 0.107**	**3.1 ± 1.3**
Cairo	116	**0.414 ± 0.067**	**5.0 ± 0.8**
Chengdu	73	**1.248 ± 0.221**	**8.0 ± 1.4**
Chicago	113	**−0.684 ± 0.191**	**−5.1 ± 1.4**
Chongqing	67	**1.529 ± 0.290**	**10.2 ± 1.9**
Damascus	115	**0.185 ± 0.089**	**3.1 ± 1.5**
Delhi	112	0.125 ± 0.110	1.4 ± 1.2
Dhaka	107	**0.525 ± 0.063**	**10.3 ± 1.2**
Guangzhou	91	−0.252 ± 0.417	−0.8 ± 1.4
Ho Chi Minh City	108	0.049 ± 0.044	1.4 ± 1.3
Hong Kong	105	−0.424 ± 0.282	−2.5 ± 1.7
Houston	107	**−0.540 ± 0.157**	**−5.4 ± 1.6**
Hyderabad	109	**0.142 ± 0.056**	**4.7 ± 1.9**
Istanbul	108	−0.047 ± 0.230	−0.4 ± 1.9

ACPD
14, 24311–24348, 2014

Table 3. Continued.

City	N	Absolute Trend	Relative Trend
Jakarta	108	−0.241 ± 0.150	−2.1 ± 1.3
Jeddah	115	0.102 ± 0.086	1.6 ± 1.3
Johannesburg	111	**−0.488 ± 0.193**	**−3.1 ± 1.2**
Kabul	110	**0.299 ± 0.046**	**14.3 ± 2.2**
Karachi	113	**0.194 ± 0.064**	**4.0 ± 1.3**
Khartoum	116	0.018 ± 0.035	1.5 ± 2.9
Kinshasa	80	0.036 ± 0.035	1.5 ± 1.4
Kolkata	109	**0.114 ± 0.063**	**2.6 ± 1.4**
Lagos	83	**0.265 ± 0.050**	**7.8 ± 1.5**
Lahore	113	**0.334 ± 0.087**	**6.0 ± 1.6**
Lima	75	**0.363 ± 0.108**	**6.9 ± 2.0**
London	107	−0.255 ± 0.205	−1.7 ± 1.4
Los Angeles	113	**−1.656 ± 0.308**	**−5.8 ± 1.1**
Madras	106	**0.151 ± 0.058**	**3.9 ± 1.5**
Manila	102	**−0.363 ± 0.074**	**−6.0 ± 1.2**
Melbourne	111	−0.103 ± 0.082	−1.6 ± 1.3
Mexico City	104	−0.354 ± 0.276	−1.3 ± 1.0
Moscow	95	−0.185 ± 0.273	−1.2 ± 1.8
Mumbai	103	0.037 ± 0.077	0.6 ± 1.2
Nagoya	101	−0.400 ± 0.244	−2.3 ± 1.4
Nairobi	88	**0.172 ± 0.040**	**13.1 ± 3.0**
New York	113	**−0.950 ± 0.310**	**−4.3 ± 1.4**
Osaka	110	**−0.445 ± 0.231**	**−2.7 ± 1.4**
Paris	108	**−0.471 ± 0.171**	**−3.3 ± 1.2**
Philadelphia	109	**−0.917 ± 0.205**	**−5.9 ± 1.3**
Po Valley	112	**−0.621 ± 0.214**	**−3.4 ± 1.2**
Rhein-Ruhr	104	**−0.452 ± 0.219**	**−2.8 ± 1.4**
Rio de Janeiro	102	−0.073 ± 0.090	−0.9 ± 1.1
Riyadh	115	**0.270 ± 0.133**	**2.1 ± 1.1**

ACPD
14, 24311–24348, 2014

Table 3. Continued.

City	N	Absolute Trend	Relative Trend
San Francisco	113	**−0.442 ± 0.124**	**−5.0 ± 1.4**
Santiago	115	**0.270 ± 0.106**	**2.8 ± 1.1**
Sao Paulo	104	−0.006 ± 0.161	0.0 ± 1.0
Seoul	105	−0.576 ± 0.517	−1.9 ± 1.7
Shanghai	106	**1.306 ± 0.347**	**4.2 ± 1.1**
Shenyang	106	**1.705 ± 0.278**	**9.4 ± 1.5**
Shenzhen	101	**−0.842 ± 0.351**	**−3.8 ± 1.6**
Sydney	111	**−0.239 ± 0.116**	**−2.9 ± 1.4**
Taipei	96	0.040 ± 0.209	0.4 ± 2.1
Tehran	115	**0.634 ± 0.216**	**3.2 ± 1.1**
Tianjin	110	**2.831 ± 0.480**	**7.7 ± 1.3**
Tokyo	108	**−1.282 ± 0.306**	**−4.9 ± 1.2**
Washington	112	**−0.740 ± 0.184**	**−6.3 ± 1.6**
Wuhan	107	**1.063 ± 0.188**	**6.4 ± 1.1**

ACPD
14, 24311–24348, 2014

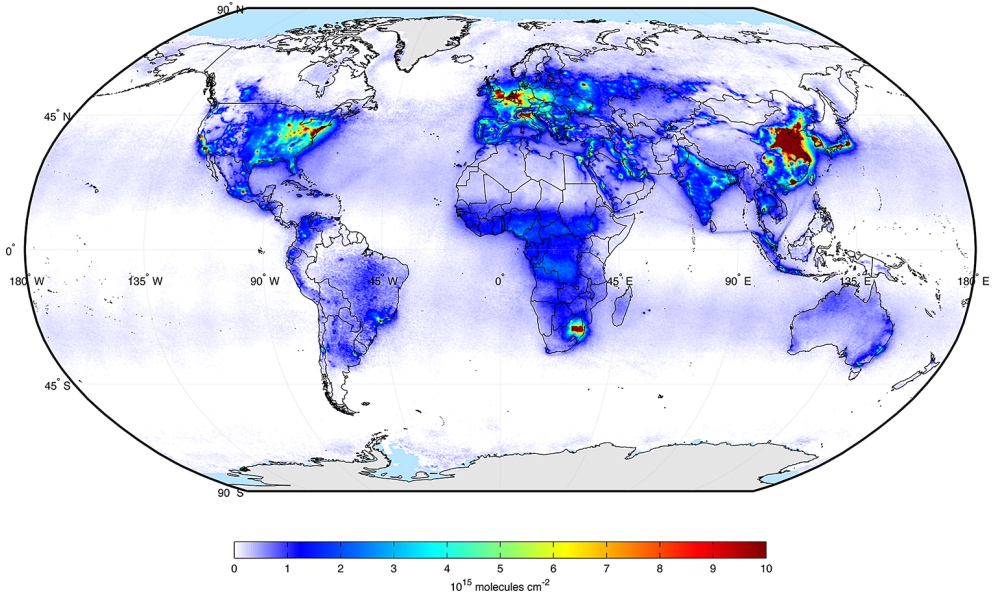

Figure 1. Global map of long-term average tropospheric NO_2 column derived from SCIAMACHY data (given in units of $\times 10^{15}$ molecules cm^{-2}). The average was computed over the entire usable time series of SCIAMACHY data ranging from August 2002 to March 2012.

ACPD
14, 24311–24348, 2014

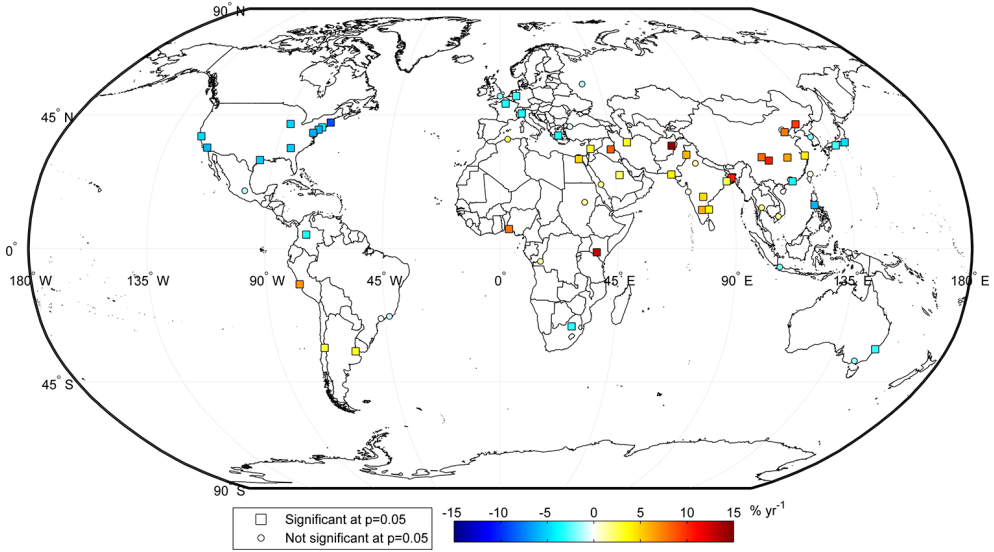

Figure 2. Global map of relative 2002–2012 tropospheric NO_2 trends over all studied urban agglomerations. The relative trends are given with respect to the long-term average concentration computed over the entire time series at each grid cell individually. The names of all the studies urban agglomerations as well as the exact absolute and relative trend values for each site can be found in Table 3.

ACPD
14, 24311–24348, 2014

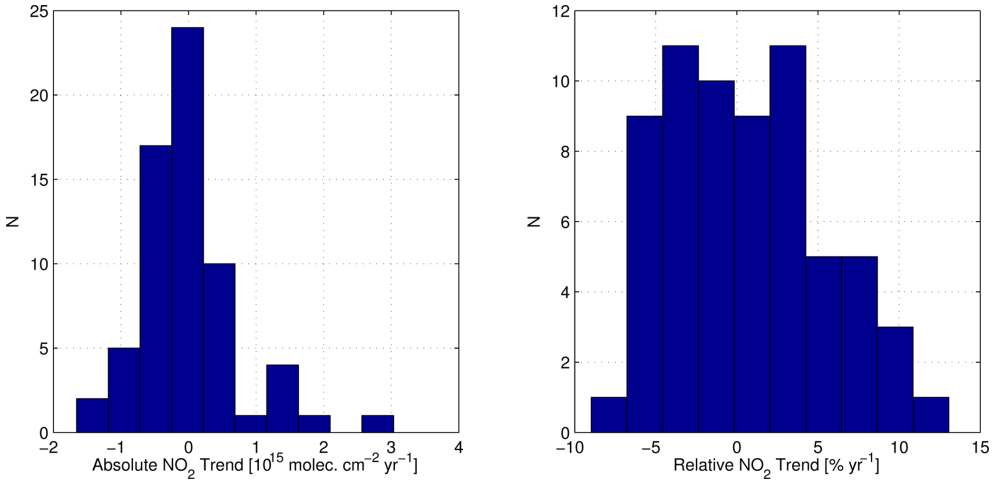

Figure 3. Histograms of absolute (left panel) and relative (right panel) tropospheric NO_2 trend over large urban agglomerations worldwide. The relative trends were computed with respect to the long-term average concentration computed over the entire time series at each grid cell individually.

ACPD
14, 24311–24348, 2014

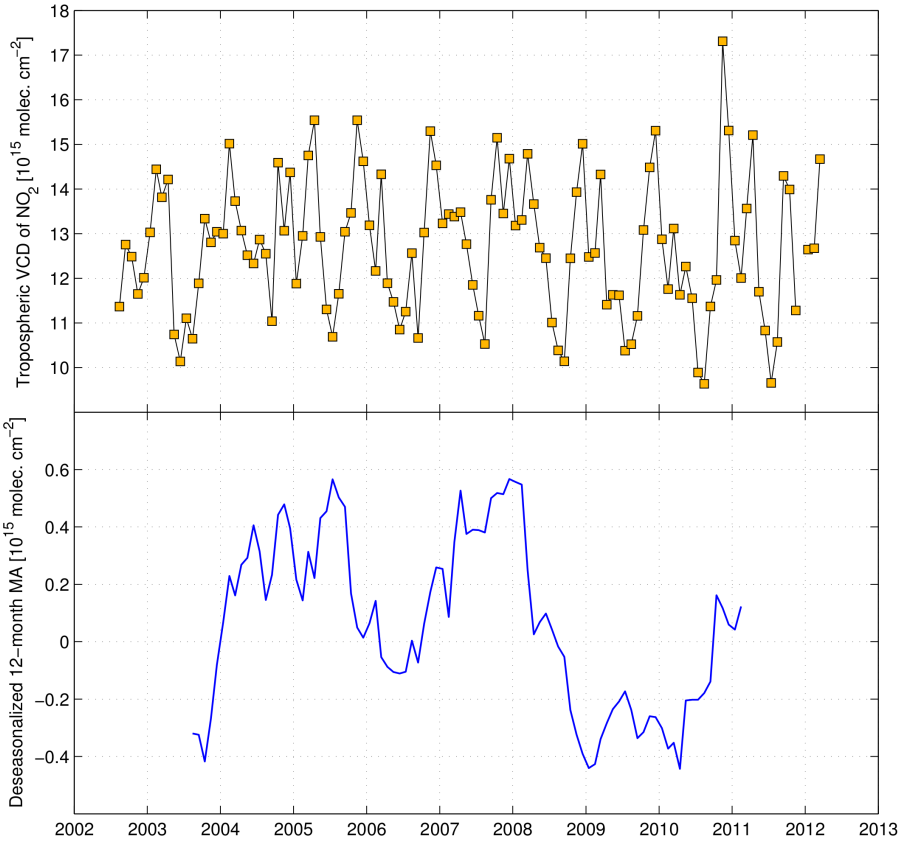

Figure 4. Average time series of SCIAMACHY-derived tropospheric NO_2 column computed over all study sites (top) and the 12-month moving average of the deseasonalized time series (bottom). In order to obtain a representative estimate, a monthly mean was only computed when at least a minimum of 40 sites provided valid data for that particular month.

ACPD
14, 24311–24348, 2014

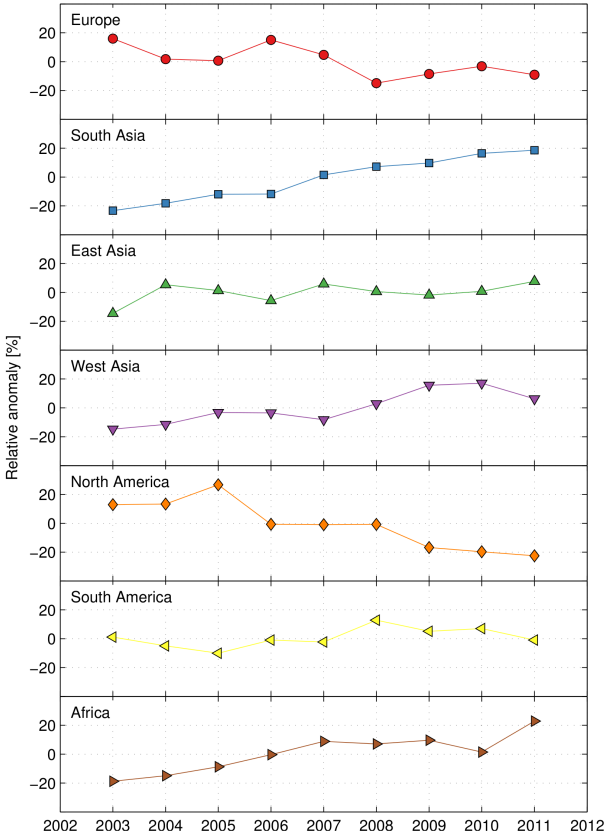

Figure 5. Interannual variability of NO_2 over large urban agglomerations, averaged by region. To facilitate an easier comparison between regions, the plot shows the average of the relative anomaly of each sites' time series within a given region. The anomalies were computed relative to the long-term mean absolute NO_2 concentration at each site.

ACPD
14, 24311–24348, 2014

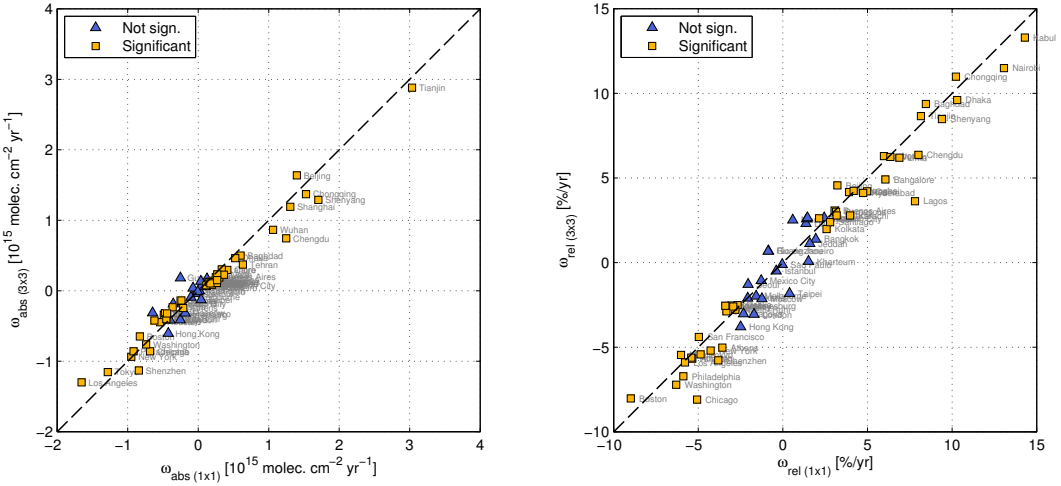

Figure 6. Comparison of absolute (left panel) and relative (right panel) trends calculated using time series extracted from a single SCIAMACHY grid cell ($\omega_{abs(1\times1)}$ and $\omega_{rel(1\times1)}$) and as the average of an array of 3×3 SCIAMACHY grid cells ($\omega_{abs(3\times3)}$ and $\omega_{rel(3\times3)}$). The markers are further distinguished into trends that are statistically significant at the $p < 0.05$ level and those that are not.

ACPD
14, 24311–24348, 2014

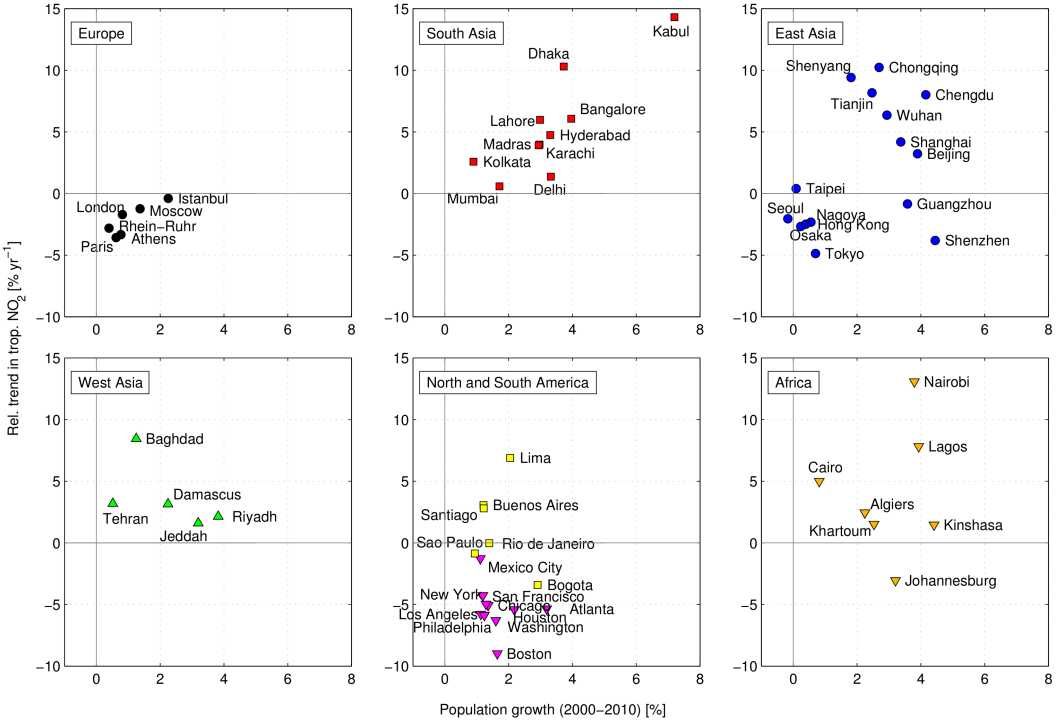

Figure 7. Relationship between population growth for the period 2000 and 2010 and SCIAMACHY-derived trends in tropospheric NO_2 for 2002 to 2012, by region.

ACPD
14, 24311–24348, 2014